Front. Mater. Sci. 2017, 11(1): 22–32
DOI 10.1007/s11706-017-0368-x

RESEARCH ARTICLE

Fabrication and characterization of *Antheraea pernyi* silk fibroin-blended P(LLA-CL) nanofibrous scaffolds for peripheral nerve tissue engineering

Juan WANG[1], Binbin SUN[1], Muhammad Aqeel BHUTTO[1], Tonghe ZHU[1], Kui YU[3], Jiayu BAO[1], Yosry MORSI[4], Hany EL-HAMSHARY[5,6], Mohamed EL-NEWEHY[5,6], and Xiumei MO (✉)[1,2]

1 State Key Laboratory for Modification of Chemical Fibers and Polymer Materials College of Chemistry, Chemical Engineering and Biotechnology, Donghua University, Shanghai 201620, China
2 Shandong International Biotechnology Park Development Co., Ltd., Yantai 264670, China
3 College of Materials Science and Engineering, Donghua University, Shanghai 201620, China
4 Faculty of Engineering and Industrial Sciences, Swinburne University of Technology, Hawthorn, Vic 3122, Australia
5 Department of Chemistry, College of Science, King Saud University, Riyadh 11451, Saudi Arabia
6 Department of Chemistry, Faculty of Science, Tanta University, Tanta 31527, Egypt

ABSTRACT: Electrospun nanofibers have gained widespreading interest for tissue engineering application. In the present study, ApF/P(LLA-CL) nanofibrous scaffolds were fabricated via electrospinning. The feasibility of the material as tissue engineering nerve scaffold was investigated *in vitro*. The average diameter increased with decreasing the blend ratio of ApF to P(LLA-CL). Characterization of ^{13}C NMR and FTIR clarified that there is no obvious chemical bond reaction between ApF and P(LLA-CL). The tensile strength and elongation at break increased with the content increase of P(LLA-CL). The surface hydrophilic property of nanofibrous scaffolds enhanced with the increased content of ApF. Cell viability studies with Schwann cells demonstrated that ApF/P(LLA-CL) blended nanofibrous scaffolds significantly promoted cell growth as compare to P(LLA-CL), especially when the weight ratio of ApF to P(LLA-CL) was 25:75. The present work provides a basis for further studies of this novel nanofibrous material (ApF/P(LLA-CL)) in peripheral nerve tissue repair or regeneration.

KEYWORDS: ApF/P(LLA-CL); electrospinning; nanofibers; scaffolds; Schwann cells; peripheral nerve tissue engineering

Contents

Received November 2, 2016; accepted December 13, 2016

E-mail: xmm@dhu.edu.cn

1 Introduction

Tissue engineering is a promising alternative for surgeons in place of prevailing radical methods like amputation or organ transplantation. Due to the inherent drawbacks of the prevailing therapeutic measures, tissue engineered cell–polymer constructs could become preferred scaffolds for tissue regeneration [1]. Current tissue engineering strategies for nerve regeneration have been focused on the development of alternative treatments for nerve repair [2]. An ideal tissue engineering scaffold should display a range of biological, morphological, chemical, physical, and mechanical properties, such as: biocompatibility; an optimum balance between hydrophilicity and hydrophobicity to allow easy cell attachment; porosity for cell migration; mimic the structure and biological functions of the natural extracellular matrix (ECM) [3]. Thus, the architecture of an engineered scaffold is very important in the design and development of implants for reconstructive surgery and other medical applications. In recent years, different methods have been used to produce nanostructured scaffolds such as electrospinning, phase separation, emulsion templating, and salt leaching [4–5]. Among the techniques, electrospinning is an effective and suitable technique for fabricating three-dimensional (3D) scaffolds because electrospinning can generate connected porous nanofibrous scaffolds with high porosity and large surface area-to-volume ratio resembling to the topographic features of the ECM [6–7]. Various biocompatible and biodegradable synthetic biomaterials such as poly (lactic-co-glycolic acid) (PLGA), poly (l-lactic acid) (PLLA), poly (caprolactone) (PCL) have been used for tissue engineering nerve scaffolds by electrospinning [8]. The main advantage of synthetic polymers is that they are available in bulk and their properties can be tailored. However, they lack cell recognition signals and sometimes their degradation products may be toxic. Consequently, a number of natural polymers like silk, collagen, keratin, elastin and chitosan are of considerable interest for scaffold fabrication by electrospinning due to their structural properties, superior biocompatibility, and unique hydrophilicity [9–14]. But there are still several drawbacks of them, such as fragility and bad tenacity which limited supply and restricted design flexibility.

Silk fibroin, a natural biopolymer produced by two species of silkworms, domestic and wild, has been used as textile material for thousands of years. Silk proteins offer several advantageous properties, including biocompatibility, non-toxic and support various cells to adhere and proliferate. As biomedical materials, such as wound dressing, tissue engineering scaffolds for skins, bones, tendons, vessels, nerves, etc., domestic silk has been widely studied in recent years [15]. However, there is limited literature regarding the application of wild silkworm silk fibroin in tissue engineering scaffolds. Chinese temperate oak tasar silkworm, *Antheraea pernyi* (*A. pernyi*), is one of the most well-known wild species among wild silkworms [16]. Compared with *Bombyx mori* silk fibroin (BSF), *A. pernyi* silk fibroin (ApF) is rich in Ala, Asp and Arg and has less Gly. In addition, the fibroin can produce superior materials due to the presence of putative cell attachment sites and the RGD sequences [17–19]. RGD (Arg-Gly-Asp), the tripeptide sequence serves as a suitable receptor and enhances the binding affinity of the cell surface receptors to achieve a specific combination of receptor-mediated endocytosis that is beneficial for cell attachment [20]. It can be proved in some research that ApF provides much stronger cell adhesion compared to collagen and BSF [21]. However, regenerated ApF possesses weak mechanical properties. In the nerve tissue engineering, electrospun scaffolds with suitable mechanical properties should mimic the nanofibrous features of ECM to maintain stability before the cells can produce their own ECM.

Poly (L-lactic acid-co-caprolactone) (P(LLA-CL)) is a copolymer of L-lactic acid and caprolactone. The synthetic biodegradable material with unique mechanical properties has hydrophobic nature that limits their use as tissue engineering scaffolds [22]. The electrospinning of ApF/P (LLA-CL) fibroin blends may obtain a new scaffold with better biocompatibility, mechanical and physiochemical properties for the nerve tissue engineering.

In the present study, the ApF/P(LLA-CL) nanofibers with different weight ratios were fabricated. The morphology, structure, mechanical strength and surface wettability properties are investigated. To evaluate possible use of the ApF/P(LLA-CL) nanofibrous scaffolds in the nerve tissue engineering, the Schwann cell (SC) proliferation and

morphology were studied on different scaffolds. The present work provides the basis for further studies of this novel nanofibrous material in nerve tissue repair or regeneration.

2 Materials and method

2.1 Materials

Non-mulberry temperate oak tasar *A. pernyi* silk cocoons were sourced from Liaoning Province, China. The co-polymer, P(LLA-CL) with the L-lactic acid/ε-caprolactone ratio of 50:50, was purchased from Jinan Daigang Bioengineering Co. Ltd., China. 1,1,1,3,3,3-Hexafluoro-2-propanol (HFIP) was acquired from Shanghai Darui Fine Chemical Co., Ltd. (Shanghai, China). The mouse SCs for *in vitro* analysis were obtained from Shanghai Institute of Biochemistry and Cell Biology (SIBCB, CAS, China). All culture media and reagents, unless stated otherwise, were purchased from Invitrogen and Sigma-Aldrich (St. Louis, MO).

2.2 Preparation of ApF

Nonmulberry temperate oak tasar *A. pernyi* silk cocoons were degummed by boiling three times in 0.2 wt.% sodium bicarbonate solution at 100°C for 30 min to extract the traces of sericin proteins and wax, followed by rinsing thoroughly with distilled water. After drying, the degummed fibers were dissolved in a 9 mol/L LiSCN solution at 50°C for 1 h. The silk solution was then dialyzed against distilled water for 4 d to remove salt at room temperature. Finally, the ApF solution was filtered and freezing-dried to obtain the regenerated ApF sponges.

2.3 Electrospinning

The electrospinning solution was prepared by dissolving ApF and P(LLA-CL) with the weight ratio of 50:50 to yield different concentrations from 6% to 12% (w/v), and 10% (w/v) ApF/P(LLA-CL) blends solution with different weight ratios of *w*(ApF):*w*(P(LLA-CL)) at 100:0, 75:25, 50:50, 25:75 and 0:100 was prepared by using the same solvent system. All prepared solutions were constantly stirred overnight. The 5 mL of each solution were pumped through 9-gauge needle with the flow rate of 1.5 mL/h whereas the distance between the collector and syringe was set 14 cm. A high voltage of 14 kV was supplied (BGG6-358, BMEI Co. Ltd., Beijing, China). The nanofibers were collected by using the ground collector. Then these scaffolds were treated by water vapor.

2.4 Morphology of electrospun nanofibers

The surface morphology of the prepared nanofibers was observed by scanning electron microscopy (SEM) at an accelerated voltage of 10 kV. Finally, according to SEM Image 100 nanofibers were selected randomly and estimated by using image analysis software (National Institute of Health, USA). Then the mean fiber diameter and the average diameter (AD) distribution of the electrospun nanofibers were calculated.

2.5 Characterization of electrospun nanofibers

The characterization of prepared scaffold was evaluated by attenuated total reflectance Fourier transform infrared spectroscopy (ATR-FTIR) as reported earlier [23]. FTIR spectra were obtained using a Nicolet 6700 Fourier transform infrared spectrometer (Thermo Fisher, USA) in the spectral region of 500–4000 cm^{-1}. The ^{13}C CP-MAS NMR spectra of the electrospun scaffolds were acquired on nuclear magnetic resonance (NMR) spectrometer (Bruker AV400, Switzerland) with a ^{13}C resonance frequency of 100 MHz, contact time of 1.0 ms, pulse delay time of 4.0 s. The water contact angle measurements were tested to find the surface wettabilities of the electrospun scaffolds by using a contact angle measurement instrument (OCA40, Dataphysics, Germany). The measurement used distilled water as the reference liquid and was automatically dropped onto the electrospun scaffolds. The contact angle was measured 5 times from different positions on each sample and an average value was calculated by statistical method.

Mechanical properties of the electrospun samples (10 mm × 30 mm) were tested by a materials testing machine (H5K-S, Hounsfield, UK) at an ambient temperature of 20°C with 65% humid environment and a elongation speed of 10 mm/min. Each sample was measured 5 times and tensile strength and elongation were calculated.

2.6 SCs culture and seeding

The rat SCs were used to study the cell proliferation and morphology on different scaffolds. The cells were cultured in Dulbecco's modified Eagle's medium (DMEM) containing 10% fetal bovine serum (FBS) and 1% penicillin in a humidified atmosphere with 5% CO_2 at 37°C. The media

were changed on every 2nd day. Before cell seeding, the scaffolds were sterilized with 75% ethanol for 24 h, and then washed three times with phosphate buffer saline (PBS) in super clean bench. SCs were seeded at a density of 1.0×10^4 cells per well onto the scaffolds and tissue culture plate (TCP) and then cultured for a period of 7 d.

2.7 Cell proliferation and morphology on scaffolds

The SCs were proliferated for 1, 3, 5 and 7 d on electrospun scaffolds and TCP (control), at which time point the cytoviability was determined by the 3-[4, 5-dimehyl-2-thiazolyl]-2, 5-diphenyl-2-H-tetrazo-lium bromide (MTT) assay. Each test point has performed three parallel experiments. The plate was read at the absorbance of 492 nm by an enzyme-labeled Instrument (MK3, Thermo, USA). The optical density (OD) value is proportional to the cytoviability.

Cell proliferation and morphology were studies on different scaffolds by performing paraffin embedding phalloidin and immunofluorescence staining. After 3 d of culturing, the cell-scaffolds were rinsed 3 times with PBS (3 min per wash) and fixed with 4.0% paraformaldehyde solution for 30 min. After washed 3 times with PBS, they were permeabilized in 0.1% Triton X-100 for 5 min, and then blocked in 1.0% bovine serum albumin (BSA) for 30 min. The cells were then labeled with rhodamine phalloidin and 4′,6-diamidino-2-phenylindole (DAPI) PBS solution for 30 and 5 min, respectively. The prepared samples were observed by an optical microscope (H600L, Nikon, Japan).

Cell morphology and the interaction between cells and scaffolds were also studied via SEM at the 3th day of incubation. The culture media were removed from scaffolds by gently washing with PBS, and then cells were fixed with 4% paraformaldehyde (PFA) solution for 30 min at 4°C. Then the prepared scaffolds were dehydrated using ethanol with concentrations of 30%, 50%, 70%, 90% and 100% (v/v) respectively, before being dried. Subsequently, the samples were gold sputter-coated to prevent charging during SEM imaging.

2.8 Statistical analysis

Statistical analysis was performed using origin 8.5 (Origin Lab Inc., USA). All the values were in triplicate and expressed as means ± standard deviation (SD). Statistical comparisons were determined by the analysis of one-way analysis of variance (ANOVA). Data with p-values < 0.05 were considered as statistically significant.

3 Results and discussion

3.1 Morphology of electrospun nanofibers

It reported that the solution concentration plays a dominant role in determining the nanofiber morphology, diameter and distribution [24]. Previously it is reported that under the same electrospinning parameters if solution concentration is changed it effects on diameter of nanofibers [25–26]. To confirm the effects of the ApF/P(LLA-CL) solution concentration on morphology, diameter and distribution, SEM images were obtained. Figure 1 showed the surface morphology and diameter distribution of electrospun ApF/P(LLA-CL) (w(ApF):w(P(LLA-CL)) = 50:50) blend nanofibers at different concentrations from 6% to 12% (w/v). It can be seen that uniform and smooth nanofibers could be obtained when the concentration of the blended ranged from 6% to 12%. From numerical statement of the AD and the SD, the nanofiber AD gradually increased from 180 to 838 nm. The results indicated that as the concentration of solution increases, the fiber diameter increases sharply. It may be that the electrospinning jet with lower polymer concentration gives thinner fiber after HFIP solvents evaporated during electrospinning. Increasing concentration leads to heavy polymer chain entanglements. Similar results are reported for the polyether sulfone and nylon nanofibers [24,27].

To confirm the effect of the weight ratio of w(ApF):w(P(LLA-CL)) on morphology, the electrospun ApF/P(LLA-CL) nanofibers with different blend weight ratios of w(ApF):w(P(LLA-CL)) from 100:0 to 0:100 were fabricated. The surface morphology, diameter distribution and structure of such electrospun fibers were observed via SEM (Fig. 2). The morphology of electrospun fibers changed from a bead shape (Fig. 2(a)) to a uniform cylindrical shape (Figs. 2(b)–2(e)) with increasing the content of P(LLA-CL). It is known that a critical concentration and viscosity of natural polymer solution needs to be exceeded for electrospinning, because below such a concentration and viscosity, chain entanglements of the polymer are insufficient to stabilize the jet, and a bead-like structure in the fiber tends to forms [28]. It was demonstrated that the scaffolds have many 3D structures. It was reported that higher porosity provided space for cell to proliferation and enhanced the nutrition transport [29]. It was noted that the

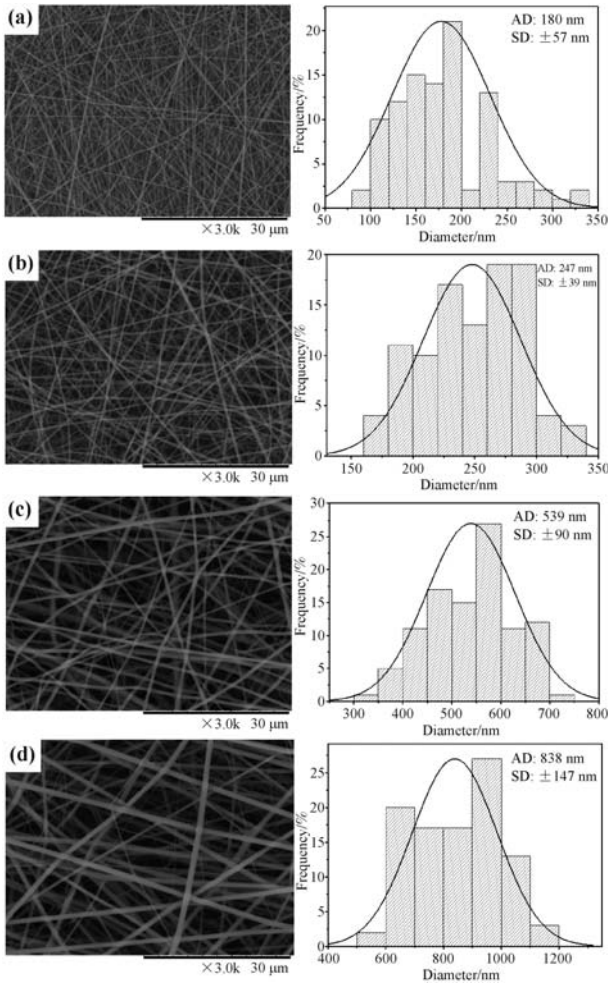

Fig. 1 SEM images and diameter distributions of electrospun ApF/P(LLA-CL) (50:50) blend nanofibers at different concentrations: **(a)** 6% (w/v); **(b)** 8% (w/v); **(c)** 10% (w/v); **(d)** 12% (w/v).

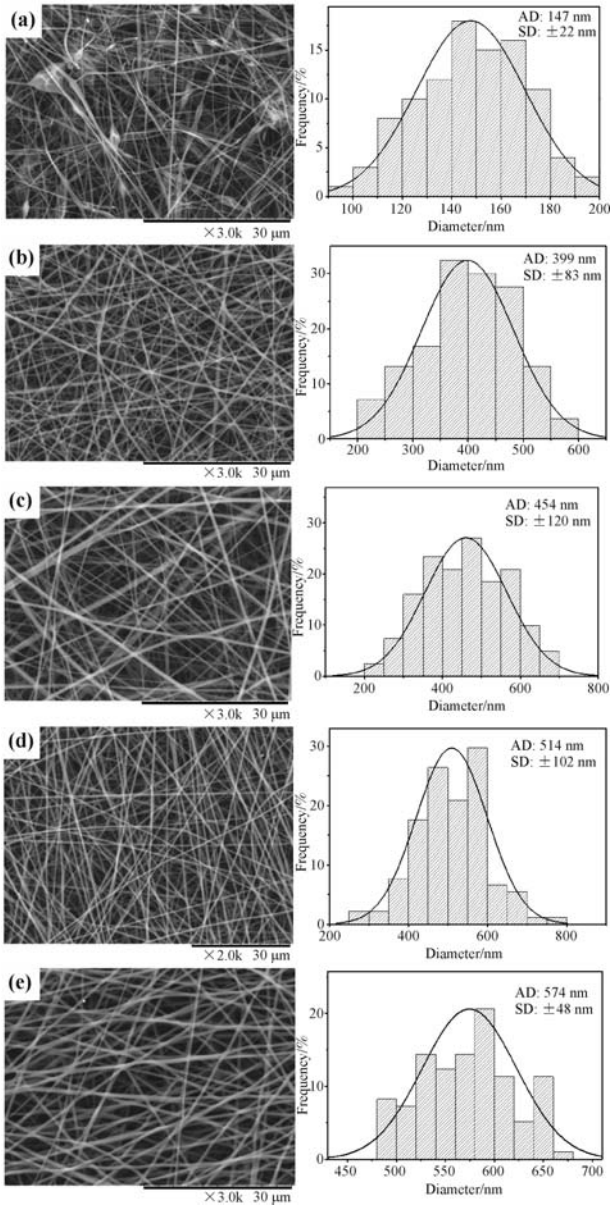

Fig. 2 SEM images and diameter distributions of 10% (w/v) ApF/P(LLA-CL) solution with different blend weight ratios of *w*(ApF):*w*(P(LLA-CL)): **(a)** 100:0; **(b)** 75:25; **(c)** 50:50; **(d)** 25:75; **(e)** 0:100.

nanofiber AD gradually increased from 399 to 574 nm with decreasing the ApF content in the blend. It may be due to the decrease of conductivity of the blend solution with decreasing the ApF content. ApF is a typical amphiprotic macromolecule electrolyte. The ApF chains are composed of 80 alternately arranged hydrophobic ploy alanine block (PAB) and hydrophilic non-ploy alanine block (NPAB) regions [30]. ApF contains more polar amino acids than BSF. The ratios of polar to nonpolar polar amino acids in ApF and BSF are 0.33 and 0.27, respectively [31], which shows that ApF is more conductive that influenced on exertion of fiber jet and produces a smaller fiber [32].

3.2 FTIR and ^{13}C CP/MAS NMR analysis

The chemical characteristics of the electrospun nanofibers were determined by ATR-FTIR. Figure 3(a) shows ATR-FTIR spectra (4000–500 cm^{-1}) of ApF/P(LLA-CL) blended nanofibers. The main characteristic peak of pure ApF (Curve i in Fig. 3(a)) and ApF/P(LLA-CL) with other different weight ratios (Curves ii–v in Fig. 3(a)) was noted at 3295 cm^{-1}, which represents to N – H and hydroxyl O – H, corresponding of the stretching vibration of free amino acid group. It implies the presence of ApF in the ApF/P(LLA-CL) scaffold. The representative adsorption peak at 3069 cm^{-1} is corresponding to $-CH_3$ stretching vibrations in pure ApF. However, the absorption bands gradually weakened with decreasing the *w*(ApF):*w*(P(LLA-CL)) ratio of ApF. The absorption band at

2938 cm^{-1} ($-CH_2$) was observed in ApF, P(LLA-CL) and ApF/P(LLA-CL) with other different weight ratios. P (LLA-CL) and ApF/P(LLA-CL) scaffolds have adsorption peaks at 1756 cm^{-1} which is corresponding to the C–O stretching [33]. Significant absorption bands at 1630 cm^{-1} (amide I), 1520 cm^{-1} (amide II) and 960 cm^{-1} (amide IV) appeared in pure ApF and ApF/P(LLA-CL) scaffolds. These absorption bands are characteristic of the β-sheet structure [34]. These results indicated that ApF/P(LLA-CL) blended nanofibrous scaffolds with different weight ratios were of no obvious difference, and showed characteristic peaks of both ApF and P(LLA-CL).

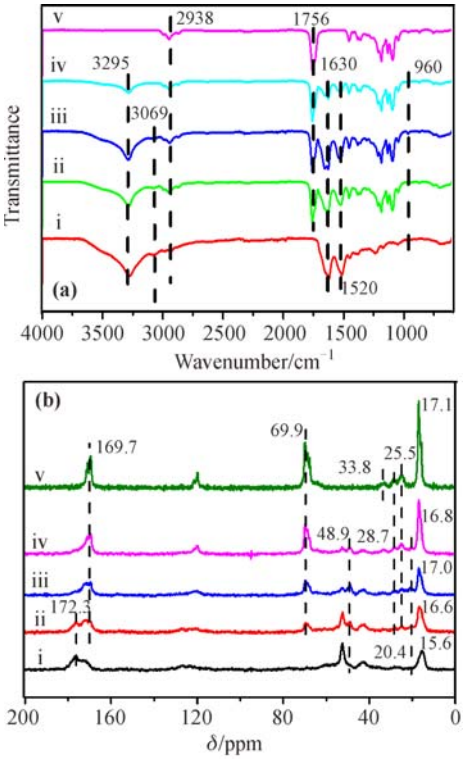

Fig. 3 Structural analyses of ApF/P(LLA-CL) blended nanofibers (100:0 (i); 75:25 (ii); 50:50 (iii); 25:75 (iv); 0:100 (v)): **(a)** ATR-FTIR spectra; **(b)** ^{13}C CP/MAS NMR spectra.

The solid-state ^{13}C CP/MAS NMR spectroscopy has been applied successfully to the structure analytical of polymers including proteins because the isotropic chemical shifts of carbon atomic in proteins are strongly related to the secondary structure. The ^{13}C NMR spectra of pure ApF, P(LLA-CL) and ApF/P(LLA-CL) nanofibrous scaffolds were shown in Fig. 3(b). In ^{13}C NMR spectra of P(LLA-CL) nanofibrous scaffolds (Curve i in Fig. 3(b)), peak at 169.7 ppm was assigned to carbonyl carbons, peaks at 17.1 and 69.9 ppm were assigned to methyl, methane of LLA, and peaks at 33.8, 28.7 and 25.5 ppm were assigned to methylene of CL with two carbons (C_3 and C_4) resonating at the same frequency, 25.5 ppm [35–36]. The relationships between the conformation and ^{13}C chemical shift for Ala, a major amino acid residue of ApF, were well established [37]. The ^{13}C chemical shifts were 20.4 ppm for Ala Cβ, 48.9 ppm for Ala Cα, and 172.3 ppm for Ala C=O [31]. The ^{13}C NMR spectra of ApF/P(LLA-CL) blended nanofibrous scaffolds with different weight ratios were of no difference, and showed characteristic chemical shifts of both ApF and P(LLA-CL). These results indicated that ApF and P(LLA-CL) had no obvious chemical bond reaction, and the conformation of ApF in ApF/P(LLA-CL) blended nanofibrous scaffolds with different weight ratios took mainly β-sheet, in accordance with the results from the FTIR spectra. It also demonstrated that ApF protein still maintained its biological functional groups for cell recognition sites in ApF/P(LLA-CL) blended nanofibrous scaffolds.

3.3 Water contact angle analysis

Surface wettability properties of biomaterials are very important because it influences on cell adhesion, proliferation, migration and viability of many different cells [38–40]. To clarify the effect of the ApF content on surface properties of ApF/P(LLA-CL) blended nanofibrous scaffolds with different weight ratios, water contact angle was measured and the results are shown in Fig. 4. It is seen that the pure ApF nanofibrous scaffold surface was ultra-hydrophilicity (36.18°) because of its hydrophilic groups. However, the contact angle of pure P(LLA-CL) nanofibrous scaffold was 112.8°, indicating that P(LLA-CL) nanofibrous scaffold was hydrophobic. With varying the weight ratio of *w*(ApF):*w*(P(LLA-CL)) from 25:75 to 75:25 in ApF/P(LLA-CL) blended nanofibrous scaffolds, the contact angle decreased from 83.84 to 55.44. These results indicated that the addition of ApF could enhance the hydrophilicity of ApF/P(LLA-CL) blended nanofibrous scaffolds. It is reported that hydrophilic surfaces displayed better affinity for cells but lower absorption for proteins than those of hydrophobic surfaces [40]. Therefore, the hydrophilic/hydrophobic balance of the scaffold surface is very important for the further cell attachment activity and protein absorption.

3.4 Mechanical properties analysis

Mechanical properties of nanofibrous scaffolds play a critical role in application, as it need to provide an initial

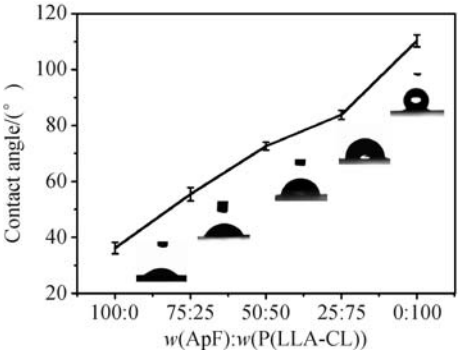

Fig. 4 Water contact angle measurement on electrospun nanofibers surface of ApF/P(LLA-CL) blended nanofibrous scaffolds with different *w*(ApF):*w*(P(LLA-CL)) ratios.

biomechanical profile for the cells before new tissue can be formed [41]. The mechanical properties of ApF/P(LLA-CL) blended nanofibrous scaffolds were characterized by tensile measurement. Figure 5 represents mechanical parameters of ApF/P(LLA-CL) blended nanofibrous scaffolds with different weight ratios, including the stress–strain curve, tensile strength and elongation at break. Pure ApF (*w*(ApF):*w*(P(LLA-CL)) = 100:0) nanofibrous scaffolds were typical brittle fracture, so the data is not shown. As shown in Fig. 5(a), all samples exhibit a linear elastic behavior. With varying the blend ratio of *w*(ApF):*w*(P(LLA-CL) in the range from 75:25 to 25:75, nanofibrous scaffolds transformed from brittle to flexible and elongation at break obviously increased from (10.5±4.21)% to (106.98±6.21)% (Fig. 5(b)). Meanwhile, the average tensile strength exhibited the variable trend, decreased from (10.23±1.52) to (5.62±0.54) MPa then increased to (8.38±2.24) MPa (Fig. 5(c)). Although pure P(LLA-CL) had excellent flexibility which elongation at break was (314.71±12.54)% (Fig. 5(b)) and the average tensile strength was (9.61±1.82)% (Fig. 5(c)), the blended nanofibers are still relative elastic and suitable for nerve tissue engineering. Further, the mechanical properties could readily be tailored to meet the requirement of peripheral nerve tissue engineering application through changing the blend ratio of ApF to P(LLA-CL).

3.5 Cell proliferation and morphology on nanofibrous scaffolds

It was reported that scaffolds for tissue engineering approaches are typically designed to promote cell growth, physiological functions and maintain normal states of cell differentiation [42]. SCs play a vital role in peripheral nerve regeneration. In order to evaluate cell viability of

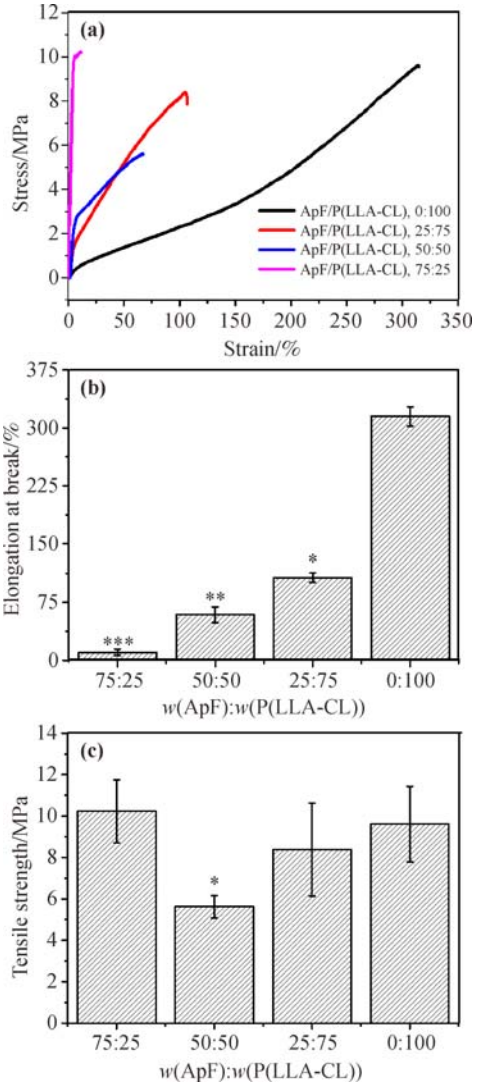

Fig. 5 Mechanical properties of ApF/P(LLA-CL) blended nanofibrous scaffolds with different *w*(ApF):*w*(P(LLA-CL)) ratios: **(a)** tensile stress–strain relationship; **(b)** elongation at break; **(c)** tensile strength. The data represent the mean ± SD (n = 5), and the symbol "*" represents statistically significant differences ($p < 0.05$) compared with pure P(LLA-CL) (*w*(ApF):*w*(P(LLA-CL)) = 0:100).

ApF/P(LLA-CL) blended nanofibrous scaffolds with different ratios, SCs were seeded on the nanofibrous scaffolds. The proliferation of SCs on different nanofibrous scaffolds and TCP was analyzed by using the MTT assay. As shown in Fig. 6, all nanofibrous scaffolds had good cell viability and there was no significant difference among them at days 1 and 3. On days 5 and 7, SCs proliferated significantly on ApF/P(LLA-CL) when *w*(ApF):*w*(P(LLA-CL)) = 25:75 compared to those of other different weight ratios and TCP ($p < 0.05$). The results reveal that these blended nanofibrous scaffolds could promote SCs growth and proliferation in comparison with pure P(LLA-CL) and

ApF. Meanwhile, among the blended nanofibrous scaffolds, ApF/P(LLA-CL) with the weight ratio of 25:75 nanofibrous scaffolds are more beneficial to SCs alignment and proliferation. This might be caused by the introduction of natural biopolymer, ApF, which has been proven to be biocompatible and facilitate cells to adhere and proliferate with its RGD sequence. It is recognized that the behavior of the attachment and proliferation of cells on scaffolding materials for tissue engineering strongly depend on the scaffold characteristics such as biocompatibility and unique hydrophilicity. Meanwhile, the existence of P(LLA-CL) in ApF/P(LLA-CL) nanofibrous scaffolds enhance the mechanical property, which exert effect on cell growth, migration and maintain stability of nanofibrous scaffolds.

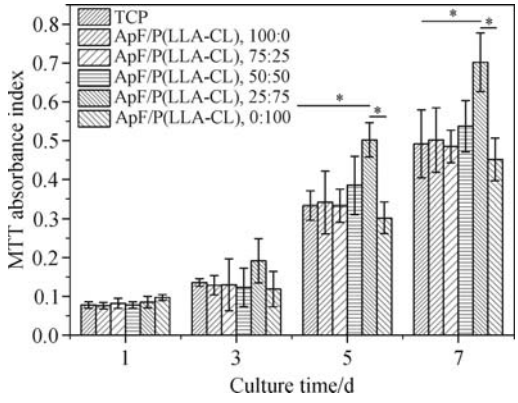

Fig. 6 Proliferation of SCs cultured on different nanofibrous scaffolds for 1, 3, 5 and 7 d. Data are expressed as mean ± SD (n = 3). The symbol "*" represents statistically significant differences ($p < 0.05$).

The SC morphology and the interaction between cells and nanofibrous scaffolds were studied for 3 d, and SEM images were shown in Fig. 7. It was observed that SCs show good cell interaction on ApF/P(LLA-CL) nanofibrous scaffolds as compared to TCP. Notably on pure P(LLA-CL) (w(ApF):w(P(LLA-CL)) = 0:100) nanofibers, SCs grow in dispersed form, which may be due to the hydrophobic properties that makes cells not properly adhere to the surface. In contrast, SCs more easily spread their cytoplasm on the surface of pure ApF (w(ApF):w(P(LLA-CL)) = 100:0) and ApF/P(LLA-CL) nanofibrous scaffolds. Meanwhile, the immunofluorescence staining images confirmed the same trend as SCs tended to spread better on surfaces of pure ApF and blended nanofibrous scaffolds than on pure P(LLA-CL) surfaces (Fig. 8). The cytoskeleton and nuclei of SCs exhibited elongated morphology on these nanofibrous scaffolds. However, the SCs on the pure P(LLA-CL) nanofibrous scaffolds showed low numbers of cells as compared to others (Fig. 8). It was because that the existence of natural material (ApF) exposed more bioactive functional groups and thus improved the interaction between scaffolds and SCs. The results indicated that the ApF/P(LLA-CL) nanofibrous scaffolds are more beneficial to SCs spread. Therefore, ApF/P(LLA-CL) nanofibrous scaffolds have potential application in peripheral nerve tissue engineering.

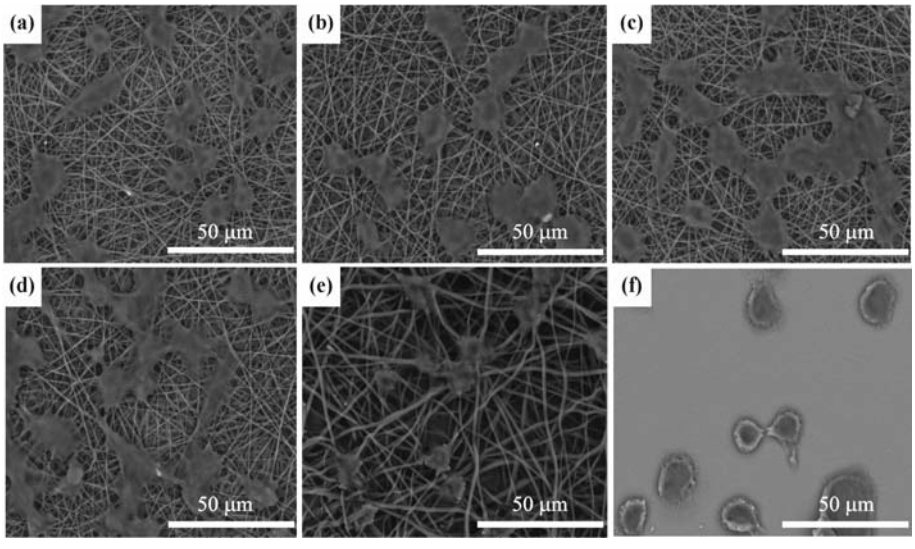

Fig. 7 SEM images of SCs grown for 3 d on ApF/P(LLA-CL) nanofibrous scaffolds and TCP with different w(ApF):w(P(LLA-CL)) ratios: **(a)** 100:0 (pure ApF); **(b)** 75:25; **(c)** 50:50; **(d)** 25:75; **(e)** 0:100 (pure P(LLA-CL)); **(f)** TCP.

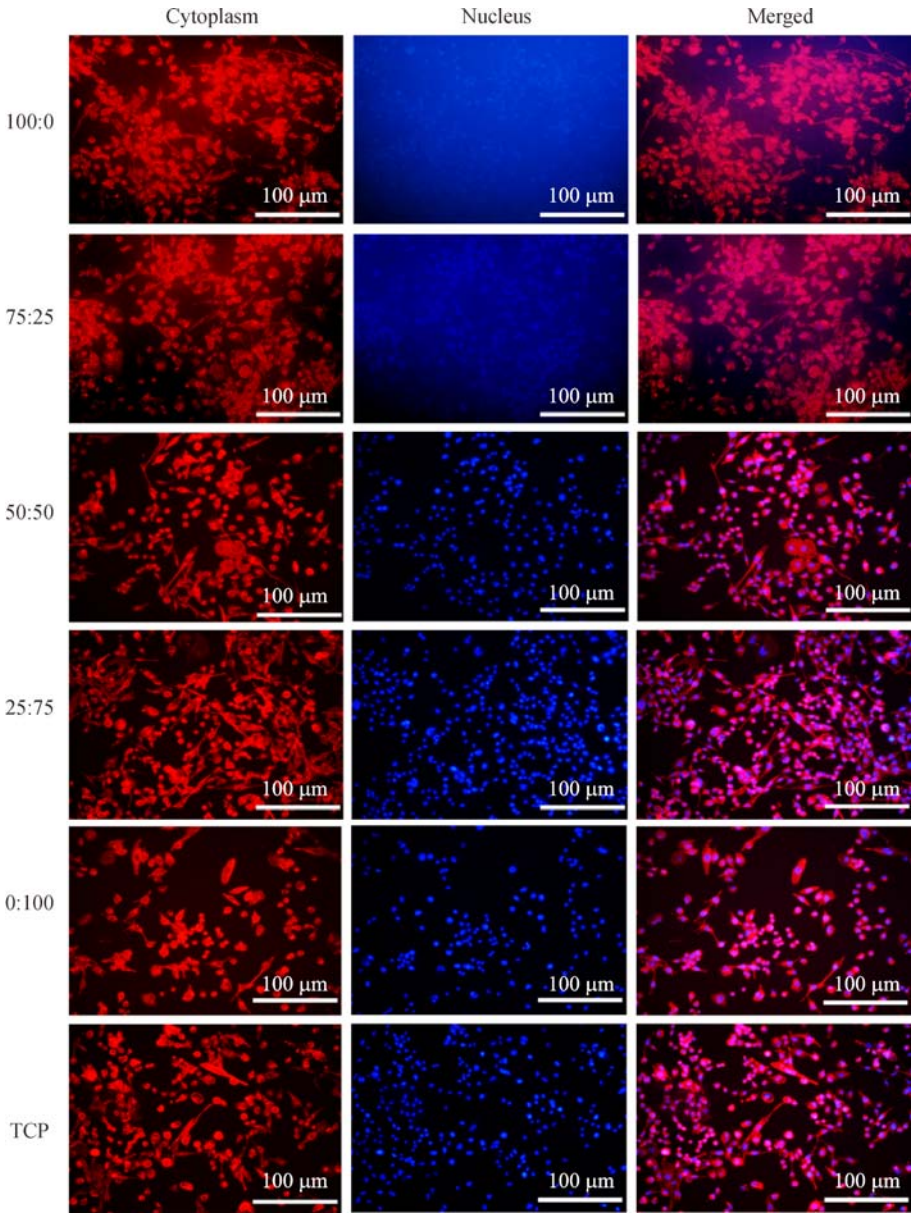

Fig. 8 Immunochemistry staining images of SCs after a 3-day culture on different nanofibrous scaffolds. Nucleus was stained by DAPI (blue) and cytoplasm was stained by rhodamine phalloidin (red).

4 Conclusions

The present study focuses on the combination of ApF with P(LLA-CL) to fabricate electrospun nanofiber mashers with well inherited excellent characteristic of ApF and P(LLA-CL). The blended nanofibrous scaffolds offered greater hydrophilicity than pure P(LLA-CL) and superior mechanical properties to ApF nanofibrous scaffolds. Blended nanofibrous scaffolds promoted SCs growth in comparison with pure P(LLA-CL), especially when w(ApF):w(P(LLA-CL)) = 25:75. This type of scaffolds may have the potential of applications in peripheral nerve tissue engineering and other related areas. The present work provides a basis for further studies of this novel nanofibrous material in nerve tissue repair or regeneration.

Acknowledgements This research was supported by the National Key Research Program of China (2016YFA0201702 of 2016YFA0201700), the National Natural Science Foundation of China (Grant Nos. 31470941 and 31271035), the Science and Technology Commission of Shanghai Municipality (Grant Nos. 15JC1490100 and 15441905100), the Ph. D. Programs Foundation of Ministry of Education of China (Grant No. 20130075110005), and the Yantai Double Hundred Talent Plan. The authors extend their appreciation to the International Scientific Partnership Program ISPP at King Saud University for funding this research work through ISPP# 0049.

References

[1] Yuksel E, Choo J, Wettergreen M, et al. Challenges in soft tissue engineering. Seminars in Plastic Surgery, 2005, 19(3): 261–270

[2] Wang C Y, Liu J J, Fan C Y, et al. The effect of aligned core–shell nanofibres delivering NGF on the promotion of sciatic nerve regeneration. Journal of Biomaterials Science: Polymer Edition, 2012, 23(1–4): 167–184

[3] Beachley V, Wen X. Polymer nanofibrous structures: Fabrication, biofunctionalization, and cell interactions. Progress in Polymer Science, 2010, 35(7): 868–892

[4] Sabbatier G, Larrañaga A, Guay-Bégin A A, et al. Design, degradation mechanism and long-term cytotoxicity of poly(l-lactide) and poly(lactide-co-ε-caprolactone) terpolymer film and air-spun nanofiber scaffold. Macromolecular Bioscience, 2015, 15 (10): 1392–1410

[5] Kim M S, Lee M H, Kwon B J, et al. Enhancement of human mesenchymal stem cell infiltration into the electrospun poly (lactic-co-glycolic acid) scaffold by fluid shear stress. Biochemical and Biophysical Research Communications, 2015, 463(1–2): 137–142

[6] Li D, Xia Y. Electrospinning of nanofibers: Reinventing the wheel? Advanced Materials, 2004, 16(14): 1151–1170

[7] Reneker D H, Chun I. Nanometre diameter fibres of polymer, produced by electrospinning. Nanotechnology, 1996, 7(3): 216–223

[8] Zhou H, Lawrence J G, Bhaduri S B. Fabrication aspects of PLA–CaP/PLGA–CaP composites for orthopedic applications: a review. Acta Biomaterialia, 2012, 8(6): 1999–2016

[9] Elsabee M Z, Naguib H F, Morsi R E. Chitosan based nanofibers. Materials Science and Engineering C, 2012, 32(7): 1711–1726

[10] Jayakumar R, Prabaharan M, Nair S V, et al. Novel chitin and chitosan nanofibers in biomedical applications. Biotechnology Advances, 2010, 28(1): 142–150

[11] Rnjak-Kovacina J, Wise S G, Li Z, et al. Tailoring the porosity and pore size of electrospun synthetic human elastin scaffolds for dermal tissue engineering. Biomaterials, 2011, 32(28): 6729–6736

[12] Lee K Y, Jeong L, Kang Y O, et al. Electrospinning of polysaccharides for regenerative medicine. Advanced Drug Delivery Reviews, 2009, 61(12): 1020–1032

[13] Sell S A, McClure M J, Garg K, et al. Electrospinning of collagen/biopolymers for regenerative medicine and cardiovascular tissue engineering. Advanced Drug Delivery Reviews, 2009, 61(12): 1007–1019

[14] Zhang X, Reagan M R, Kaplan D L. Electrospun silk biomaterial scaffolds for regenerative medicine. Advanced Drug Delivery Reviews, 2009, 61(12): 988–1006

[15] Tao W, Li M, Zhao C. Structure and properties of regenerated *Antheraea pernyi* silk fibroin in aqueous solution. International Journal of Biological Macromolecules, 2007, 40(5): 472–478

[16] Liu Y, Li Y, Li X, et al. The origin and dispersal of the domesticated Chinese oak silkworm, *Antheraea pernyi*, in China: a reconstruction based on ancient texts. Journal of Insect Science, 2010, 10(1): 180

[17] Kundu S C, Kundu B, Talukdar S, et al. Nonmulberry silk biopolymers. Biopolymers, 2012, 97(6): 455–467

[18] Patra C, Talukdar S, Novoyatleva T, et al. Silk protein fibroin from *Antheraea mylitta* for cardiac tissue engineering. Biomaterials, 2012, 33(9): 2673–2680

[19] Yukuhiro K, Kanda T, Tamura T. Preferential codon usage and two types of repetitive motifs in the fibroin gene of the Chinese oak silkworm, *Antheraea pernyi*. Insect Molecular Biology, 1997, 6(1): 89–95

[20] Tian H, Lin L, Chen J, et al. RGD targeting hyaluronic acid coating system for PEI–PBLG polycation gene carriers. Journal of Controlled Release, 2011, 155(1): 47–53

[21] Minoura N, Aiba S, Higuchi M, et al. Attachment and growth of fibroblast cells on silk fibroin. Biochemical and Biophysical Research Communications, 1995, 208(2): 511–516

[22] Kim B S, Mooney D J. Development of biocompatible synthetic extracellular matrices for tissue engineering. Trends in Biotechnology, 1998, 16(5): 224–230

[23] Sun B, Li J, Liu W, et al. Fabrication and characterization of mineralized P(LLA-CL)/SF three-dimensional nanoyarn scaffolds. Iranian Polymer Journal, 2015, 24(1): 29–40

[24] Huang C, Chen S, Lai C, et al. Electrospun polymer nanofibres with small diameters. Nanotechnology, 2006, 17(6): 1558–1563

[25] Zhu Y, Zhang J, Zheng Y, et al. Stable, superhydrophobic, and conductive polyaniline/polystyrene films for corrosive environments. Advanced Functional Materials, 2006, 16(4): 568–574

[26] Jun I, Jeong S, Shin H. The stimulation of myoblast differentiation by electrically conductive sub-micron fibers. Biomaterials, 2009, 30(11): 2038–2047

[27] Christopherson G T, Song H, Mao H Q. The influence of fiber diameter of electrospun substrates on neural stem cell differentiation and proliferation. Biomaterials, 2009, 30(4): 556–564

[28] McKee M G, Wilkes G L, Colby R H, et al. Correlations of solution rheology with electrospun fiber formation of linear and branched polyesters. Macromolecules, 2004, 37(5): 1760–1767

[29] Zhang K, Wang H, Huang C, et al. Fabrication of silk fibroin blended P(LLA-CL) nanofibrous scaffolds for tissue engineering. Journal of Biomedical Materials Research Part A, 2010, 93(3): 984–993

[30] Sezutsu H, Yukuhiro K. Dynamic rearrangement within the *Antheraea pernyi* silk fibroin gene is associated with four types of repetitive units. Journal of Molecular Evolution, 2000, 51(4): 329–

338

[31] Freddi G, Gotoh Y, Mori T, et al. Chemical structure and physical properties of *Antheraea assama* silk. Journal of Applied Polymer Science, 1994, 52(6): 775–781

[32] Zong X, Kim K, Fang D, et al. Structure and process relationship of electrospun bioabsorbable nanofiber membranes. Polymer, 2002, 43(16): 4403–4412

[33] Xu Y, Wu J, Wang H, et al. Fabrication of electrospun poly(L-lactide-co-ε-caprolactone)/collagen nanoyarn network as a novel, three-dimensional, macroporous, aligned scaffold for tendon tissue engineering. Tissue Engineering Part C: Methods, 2013, 19(12): 925–936

[34] Lins L, Brasseur R. The hydrophobic effect in protein folding. FASEB Journal, 1995, 9(7): 535–540

[35] Zhong Z, Guo Q, Mi Y. Solid-state n. m. r. investigation of crosslinkable blends of novolac and poly(ε-caprolactone). Polymer, 1999, 40(1): 27–33

[36] Howe C, Sankar S, Tonelli A E. 13C n. m. r. observation of poly(l-lactide) in the narrow channels of its inclusion compound with urea. Polymer, 1993, 34(12): 2674–2676

[37] Nakazawa Y, Asakura T. High-resolution ^{13}C CP/MAS NMR study on structure and structural transition of *Antheraea pernyi* silk fibroin containing poly(L-alanine) and Gly-rich regions. Macromolecules, 2002, 35(6): 2393–2400

[38] Altankov G, Grinnell F, Groth T. Studies on the biocompatibility of materials: fibroblast reorganization of substratum-bound fibronectin on surfaces varying in wettability. Journal of Biomedical Materials Research, 1996, 30(3): 385–391

[39] De Bartolo L, Morelli S, Bader A, et al. The influence of polymeric membrane surface free energy on cell metabolic functions. Journal of Materials Science: Materials in Medicine, 2001, 12(10): 959–963

[40] Lampin M, Warocquier-Clérout R, Legris C, et al. Correlation between substratum roughness and wettability, cell adhesion, and cell migration. Journal of Biomedical Materials Research, 1997, 36(1): 99–108

[41] Chen Z G, Wang P W, Wei B, et al. Electrospun collagen–chitosan nanofiber: a biomimetic extracellular matrix for endothelial cell and smooth muscle cell. Acta Biomaterialia, 2010, 6(2): 372–382

[42] Lutolf M P, Hubbell J A. Synthetic biomaterials as instructive extracellular microenvironments for morphogenesis in tissue engineering. Nature Biotechnology, 2005, 23(1): 47–55